The Journal of Chemical Physics

Detailed crystallographic analysis of the ice V to ice XIII hydrogen-ordering phase transition

Cite as: J. Chem. Phys. **154**, 134504 (2021); https://doi.org/10.1063/5.0045443
Submitted: 26 January 2021 • Accepted: 12 March 2021 • Published Online: 01 April 2021

Christoph G. Salzmann, Alexander Rosu-Finsen, Zainab Sharif, et al.

The Journal of Chemical Physics ARTICLE scitation.org/journal/jcp

Detailed crystallographic analysis of the ice V to ice XIII hydrogen-ordering phase transition

Cite as: J. Chem. Phys. 154, 134504 (2021); doi: 10.1063/5.0045443
Submitted: 26 January 2021 • Accepted: 12 March 2021 •
Published Online: 1 April 2021

Christoph G. Salzmann,[1,a)] Alexander Rosu-Finsen,[1] Zainab Sharif,[1] Paolo G. Radaelli,[2] and John L. Finney[3]

AFFILIATIONS

[1] Department of Chemistry, University College London, 20 Gordon Street, London WC1H 0AJ, United Kingdom
[2] Department of Physics, University of Oxford, Parks Road, Oxford OX1 3PJ, United Kingdom
[3] Department of Physics and Astronomy and London Centre for Nanotechnology, University College London, Gower Street, London WC1E 6BT, United Kingdom

[a)] **Author to whom correspondence should be addressed:** c.salzmann@ucl.ac.uk

ABSTRACT

Ice V is a structurally highly complex material with 28 water molecules in its monoclinic unit cell. It is classified as a hydrogen-disordered phase of ice. Yet, some of its hydrogen-bonded water molecules display significant orientational order. Upon cooling pure ice V, additional orientational ordering cannot be achieved on the experimental time scale. Doping with hydrochloric acid has been shown to be most effective in enabling the phase transition of ice V to its hydrogen-ordered counterpart ice XIII. Here, we present a detailed crystallographic study of this phase transition investigating the effects of hydrochloric and hydrofluoric acid as well as lithium and potassium hydroxide doping. The magnitudes of the stepwise changes in the lattice constants during the phase transition are found to be more sensitive indicators for the extent of hydrogen order in ice XIII than the appearance of new Bragg peaks. Hydrofluoric acid and lithium hydroxide doping enable similar ordering processes as hydrochloric acid but with slower kinetics. The various possible space groups and ordered configurations of ice XIII are examined systematically, and the previously determined $P2_1/a$ structure is confirmed. Interestingly, the partial hydrogen order already present in ice V is found to perpetuate into ice XIII, and these ordering processes are found to be independent of pressure. Overall, the hydrogen ordering goes along with a small increase in volume, which appears to be the origin of the slower hydrogen-ordering kinetics under pressure. Heating pressure-quenched samples at ambient pressure revealed low-temperature "transient ordering" features in both diffraction and calorimetry.

INTRODUCTION

Ice V was discovered more than a century ago and is thermodynamically stable between ~0.35 and ~0.63 GPa at temperatures above the region of stability of ice II, as shown in Fig. 1(a).[1,2] Its monoclinic unit cell comprises 28 water molecules, which form 4-, 5-, 6-, 8-, 9-, 10-, and 12-membered rings through hydrogen bonding.[3,4] Originally, the hydrogen-bonded water molecules in ice V were thought to display complete orientational disorder.[5–7] Later, partial hydrogen order, which is permitted by the $A2/a$ space group of ice V, was found using neutron diffraction[8–10] and other methods.[11,12] Some of the fractional occupancies of the hydrogen sites deviate strongly from $\frac{1}{2}$, which defines complete hydrogen disorder.[9,10] It has been shown that the partial hydrogen order in ice V leads to a configurational entropy 6% lower than the Pauling entropy,[13] which is 3.38 J mol^{-1} K^{-1} for completely hydrogen-disordered phases of ice.

Figure 2(a) shows the crystal structure of ice V with its four crystallographically distinct oxygen atoms highlighted in different colors: O(1) in red, O(2) in green, O(3) in blue, and O(4) in yellow. The hydrogen sites are shown as "pie charts," where the gray slices indicate the fractional occupancies. The crystal structure is quite complex and can be described with two types of zig–zag chains that run parallel to the a axis.[3] One type of chain alternates between O(2) and O(3) atoms, whereas the other one contains only O(4). The D(16) and D(18) hydrogen sites are restricted to half occupancies by the symmetry of $A2/a$, which means that full hydrogen order is not possible in this space group. The structural complexity of ice

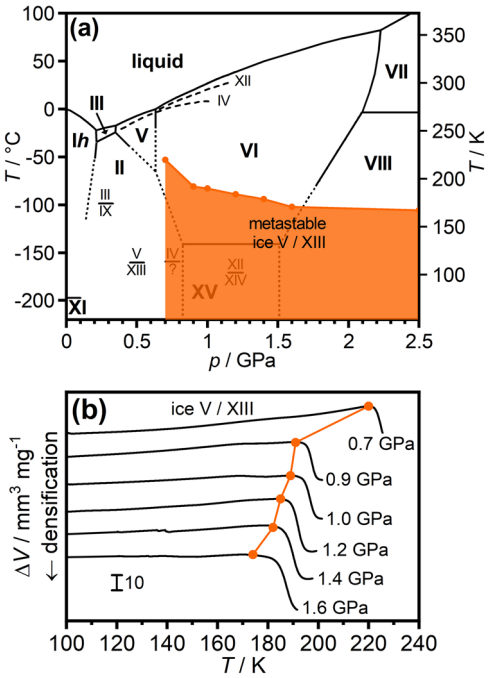

FIG. 1. (a) Phase diagram of ice with the stable phases highlighted in bold. The low-temperature metastability domain of ice V/XIII is shown as an orange-shaded area. (b) *In situ* volume changes recorded upon isobaric heating of ice V/XIII at the indicated pressures. The onset temperatures of the irreversible phase transition to ice VI are indicated by full orange circles and correspond to the ones shown in (a). The data point at 2.5 GPa was obtained using a small-diameter piston cylinder, which means that the recorded volume changes are difficult compared to the ones shown in (b) and have, therefore, been omitted.

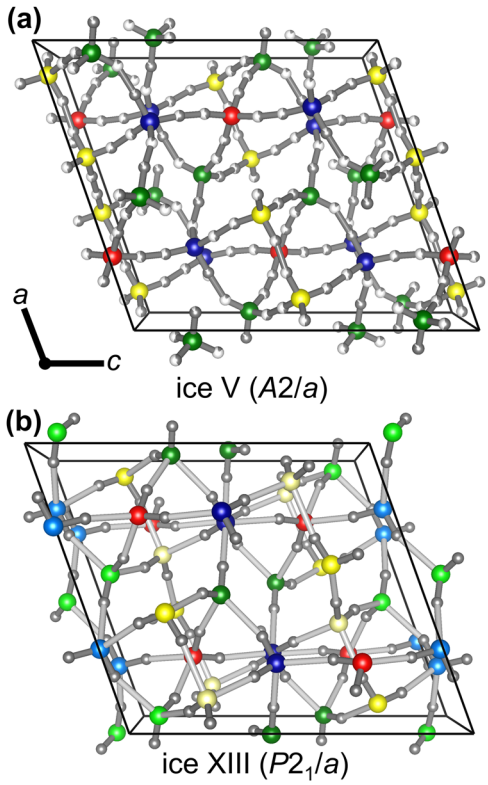

FIG. 2. Monoclinic unit cells of (a) the partially hydrogen-ordered ice V and (b) the fully hydrogen-ordered XIII.[3,10,15] Larger spheres represent the oxygen atoms and smaller spheres the hydrogen positions. For ice V, the different oxygen positions are indicated by different colors, and this color scheme is carried forward to ice XIII, where darker/lighter colors indicate the origin of the positions before Wyckoff splitting. The fully occupied hydrogen sites are shown in gray for ice XIII, whereas the gray part of the "pie chart" representation for ice V indicates the fractional occupancies of the hydrogen sites. For ice XIII, the covalent O–D bonds are shown as dark gray cylinders and the O···D bonds in light gray.

V compared to the other phases of ice also manifests in vibrational spectroscopy.[5,11,14]

Upon cooling ice V, only weak hydrogen-ordering effects can be detected.[8–12] Pure H_2O ice V displays an orientational glass transition at ~130 K corresponding to the kinetic freezing-in of the reorientation dynamics of the water molecules.[4,16] The effect of KOH doping, which was successful in hydrogen-ordering ice *Ih*,[17] was studied calorimetrically[18] and spectroscopically.[19] Handa *et al.* observed an endothermic feature in calorimetry upon heating, which was discussed in terms of a hydrogen order/disorder transition.[18] However, this could not be confirmed with Raman spectroscopy[19] and neutron diffraction.[15]

Doping with HCl on the contrary was found to be highly effective in promoting hydrogen ordering upon cooling ice V, which enabled us to discover a highly hydrogen-ordered phase named ice XIII.[15] Using neutron diffraction, we could show that the ordering phase transition is accompanied by stepwise changes in the lattice constants and a reduction of the space group symmetry from $A2/a$ to $P2_1/a$.[15,20] As shown in Fig. 2(b), the antiferroelectric structure of ice XIII comprises seven distinct oxygen positions and 14 different hydrogen bonds, which makes it by far the most structurally complex phase of ice.

The discovery of HCl as a highly effective dopant for enabling the phase transition from ice V to ice XIII has sparked several further studies. Using calorimetry, it was shown that the ice V to ice XIII phase transition at ~113 K at ambient pressure goes along with a 66% loss of Pauling entropy.[21] Considering the highly ordered nature of ice XIII, this reduced entropy change arises mainly from the partially ordered nature of ice V. According to calorimetry, the ice V to ice XIII phase transition takes place in at least two overlapping stages.[21] The phase transition was also followed with Raman spectroscopy.[22] Computationally, it was found that the structure of ice XIII proposed on the basis of neutron diffraction data is the most stable out of all the 35 possible hydrogen-ordered configurations in $P2_1/a$.[23]

HCl doping is thought to produce mobile H_3O^+ point defects that speed up molecular reorientation dynamics below the orientational glass transition of pure ice V and, hence, enable the hydrogen-ordering phase transition to take place at low temperatures. The effect of HCl doping on the dielectric relaxation times of ice V was

recently demonstrated.[24] Comparative studies of the effects of different acid dopants, such as HCl, HBr, $HClO_4$, and HF, on the hydrogen ordering of ice V found that the combination of acid strength and solubility in ice determines the effectiveness of a dopant with respect to enabling the hydrogen-ordering transition.[21,25] Further calorimetric studies investigating base dopants showed that LiOH also facilitates the hydrogen ordering of ice V.[25] Therefore, ice V is the only phase of ice that can be hydrogen-ordered with the help of both acid and base dopants. However, it should be noted that the exact structural details of the hydrogen ordering cannot be deduced from calorimetry and require neutron diffraction.

Here, we present a detailed crystallographic analysis of the ice V to ice XIII phase transition. In addition to the highly effective DCl dopant, the effects of DF, LiOD, and KOD doping on the phase transition are investigated. A particularly interesting question is if acid and base dopants promote the same type of hydrogen ordering. The previously suggested space group of ice XIII, $P2_1/a$, is re-examined, and other possibilities are discussed. Within $P2_1/a$, all possible hydrogen-ordered configurations are identified and benchmarked against the diffraction data. The hydrogen-ordered structure of ice XIII is analyzed with respect to its relationship to the partial hydrogen order that already exists in ice V. Finally, we also investigate if low-temperature "transient ordering" features can be found for ice V/XIII in both diffraction and calorimetry as they have previously been observed for ice VI/XV.[25–27]

EXPERIMENTAL

Sample preparation for neutron diffraction experiments

Doped D_2O ice V/XIII samples were prepared using 0.01 mol l^{-1} start solutions of DCl, DF, KOD, and LiOD in D_2O. The DF solutions were handled in polyethylene vials. As described in detail in Refs. 15 and 20–22, the solutions were frozen quickly by pipetting into indium cups inside piston-cylinder dies precooled to liquid-nitrogen temperature. The ice samples were then compressed to 0.5 GPa using either a hydraulic workshop press or a computerized Zwick Roell Proline Z100TN Universal Testing Machine. To achieve the conversion to ice V, the samples were heated isobarically to 250 K followed by cooling back to liquid-nitrogen temperature at cooling rates of 0.8 K min^{-1} (DCl-, DF-, and KOD-doped samples) or 2.5 K min^{-1} (LiOD doped sample). In addition to the slow-cooled samples, a DCl-doped sample was quenched at ~40 K min^{-1} under pressure using external liquid nitrogen.

Neutron diffraction experiments

The ice samples were ground using a porcelain pestle and mortar under liquid nitrogen and transferred into cylindrical vanadium cans. These were then mounted onto cryostat sticks and transferred quickly into precooled cryostats on various neutron diffraction beamlines. Excess liquid nitrogen within the vanadium cans was carefully evaporated by heating to 80 K and evacuating the cryostats. The neutron diffraction data of the slow-cooled DCl-doped sample were recorded on the GEM beamline at ISIS,[15,20] and the KOD- and DF-doped samples were characterized using the D2B instrument at the ILL. The POLARIS instrument at ISIS was used for both the quenched DCl-doped as well as the slow-cooled LiOD-doped sample. After recording data at 80 K, the samples were heated to ~130 K followed by cooling back to 80 K. The time-of-flight GEM and POLARIS instruments allowed collecting diffraction data while heating and cooling, whereas on the constant-wavelength D2B instrument, only measurements at ~80 and ~130 K were taken. The heating and cooling rates were ~0.2 K min^{-1} on the GEM and D2B instruments. On the POLARIS instrument, the quenched DCl-doped sample was heated at ~0.4 K min^{-1} followed by cooling at ~0.1 K min^{-1} and the LiOD-doped sample at ~1.2 and ~0.1 K min^{-1}, respectively. High-quality diffraction data for Rietveld analyses were recorded before and after the various heating/cooling steps, whereas the data collected during heating and cooling were of sufficient quality for determining the lattice constants. For the slow-cooled DCl-doped ice XIII sample, additional diffraction data were collected at 12 K. The Rietveld analyses were carried out using the GSAS software[28] and the crystallographic models of ices V and XIII reported in Refs. 3 and 15. The implementation of the ice rules for the fractional occupancies of the deuterium sites was achieved by using linear constraints and chemical composition restraints.

Mapping of the low-temperature metastability region of ice V/XIII and preparation of samples for calorimetry

H_2O solutions containing 0.01 mol l^{-1} HCl were used for this part. As described above, the ice V/XIII was prepared by isobaric heating at 0.5 GPa to 250 K followed by quenching. After this, the samples were reheated isobarically from 77 K at a range of different pressures between 0.7 and 2.5 GPa. The recorded volume changes of the samples are shown in Fig. 1(b) apart from the 2.5 GPa data, which were obtained using a different, small-diameter piston cylinder. The transformation of ice V to the stable ice VI is indicated by stepwise volume changes. In additional experiments, HCl-doped ice V samples were heated to ~10 K below the onset temperatures of the irreversible transformations at 1.6 and 2.5 GPa followed by quenching.

Differential scanning calorimetry (DSC)

A few small pieces of the doped high-pressure phases of ice were transferred into stainless-steel capsules with screwable lids under liquid nitrogen. These were transferred quickly into a precooled Perkin Elmer DSC 8000 advanced double-furnace differential scanning calorimeter with a base temperature of 93 K. Thermograms were recorded upon heating to 263 K at 2.5 K min^{-1} followed by cooling back to 93 K. The now ice I*h* samples were reheated at 2.5 K min^{-1} from 93 to 263 K. Finally, the moles of ice in the DSC capsules were determined by recording the endothermic melting of ice at 0 °C and using 6012 J mol^{-1} as the enthalpy of melting of H_2O ice I*h*. The thermograms of ice I*h* were subtracted from the previously recorded data as a background correction. The resulting DSC signal was divided by the number of moles of H_2O and the heating/cooling rate, which yields a quantity with J mol^{-1} K^{-1} as the unit.

RESULTS AND DISCUSSION

Changes in the lattice constants during the ice V ↔ ice XIII phase transition

Figures 3(a)–3(d) show the changes in the lattice constants upon heating and cooling the various doped ice V/XIII samples in the 80–130 K temperature range. The stepwise changes between 100 and 120 K indicate the reversible ice XIII ↔ ice V phase transition, while the magnitude of the step reflects the extent of hydrogen order in ice XIII. In line with previous Raman and calorimetry studies,[15,20–22,25] the most pronounced changes are observed for the DCl-doped ices followed by the DF- and LiOD-doped samples. For the KOD-doped sample, heating and slow-cooling lead to only very minor changes in the lattice constants, illustrating that this dopant is inefficient in enabling the phase transition. The ice XIII to ice V phase transition goes along with a contraction in the *a* lattice constant, an expansion in *b*, a quite small contraction in *c*, and a decrease in the monoclinic angle *β*. Accordingly, the most ordered ice XIII is obtained upon slow-cooling DCl-doped ice V at ambient pressure followed by the DCl-doped sample that was slow-cooled at 0.5 GPa. Anisotropy in the expansion/contraction behavior of the various lattice constants, as observed here, has also been found for the hydrogen-ordering phase transitions of ices VI/XV,[27,29] XII/XIV,[20] and III/IX.[30] It is also worth noting that in the case of the DCl, DF, and LiOD dopants, the directions of the changes for each of the lattice constants are the same, suggesting that these three dopants enable similar hydrogen-ordering processes but with different kinetics. For DCl and DF doping, this conclusion was also reached from a comparison of the isotope effect in calorimetry.[21]

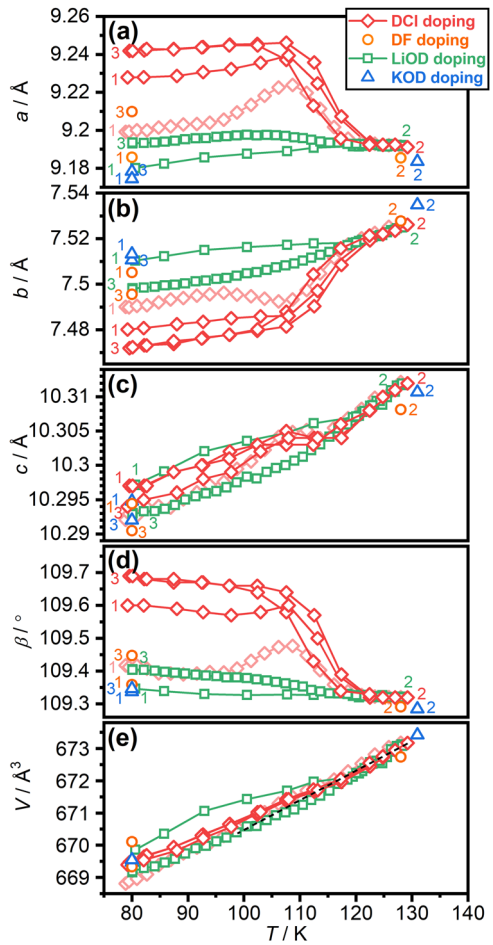

FIG. 3. (a)–(d) Lattice constants and (e) unit-cell volumes of DCl-doped (red diamonds), DF-doped (orange circles), LiOD-doped (green squares), and KOD-doped (blue triangles) ice V/XIII samples recorded upon heating at ambient pressure from ~80 to ~130 K and cooling back. The numbers indicate the sequence of heating and cooling steps. The light red diamonds represent the first heating of a pressure-quenched DCl-doped sample. All heating and cooling rates are given in the section titled "Experimental." The black dashed line in (e) highlights the small volume increase during the ice V to ice XIII phase transition based on the data from the DCl-doped sample.

Heating of the DCl-doped sample after slow-cooling under pressure leads to a small increase in the *a* lattice constant starting at ~100 K before the contraction toward ice V sets in, and similar phenomena are also observed for *b* and *β*. Such behavior has previously been observed when DCl-doped ice VI was heated at ambient pressure and has been attributed to irreversible "transient ordering" to ice XV before the reversible hydrogen disordering to ice VI sets in Ref. 27. In calorimetry, the transient ordering of ice VI upon heating manifests as an exothermic feature before the disordering endotherm.[26,31,32] The essential requirement for observing transient ordering upon heating is that the sample is metastable with respect to a more hydrogen-ordered state and that the hydrogen-ordering kinetics are sufficiently fast. As discussed later in detail, the DCl-doped sample after slow-cooling at 0.5 GPa displayed the additional Bragg peaks characteristic of ice XIII. Therefore, to prepare a more disordered and metastable sample at low temperatures, a DCl-doped ice V sample was quenched at 0.5 GPa at ~40 K min^{-1}. The lattice constants obtained upon heating this sample are indicated by light red diamonds in Figs. 3(a)–3(d). As expected, the lattice constants indicate a higher degree of disorder at 80 K compared to the slow-cooled sample. Upon heating this quite disordered sample at 0.4 K min^{-1}, extensive transient ordering can be observed in the *a*, *b*, and *β* lattice constants. However, as also observed for ice VI/XV,[27] the most ordered ice XIII is obtained by slow-cooling and not during the transient ordering.

Figure 4 shows the neutron diffraction data collected upon heating the DCl-doped and pressure-quenched ice V sample followed by slow-cooling. Focusing on the slow-cooling first, the additional Bragg peaks of ice XIII at ~2.76, ~2.22, and ~2.07 Å appear at ~115 K. Consistent with a disordered sample after quenching under pressure, these are absent in the starting material at 80 K. However, close inspection of the diffraction data upon heating reveals the appearance of weak additional Bragg intensities characteristic of ice XIII at around 112 K, which then disappear again upon further heating consistent with the disordering after the transient ordering.

The change in volume during the ice XIII to ice V phase transition is very small, as shown in Fig. 3(e). The black dashed line shows the linear extrapolation of the volume change of the DCl-doped ice V toward lower temperatures. According to this analysis, the phase transition from ice V to ice XIII goes along with a very small increase in the volume. Such an expansion in volume upon hydrogen

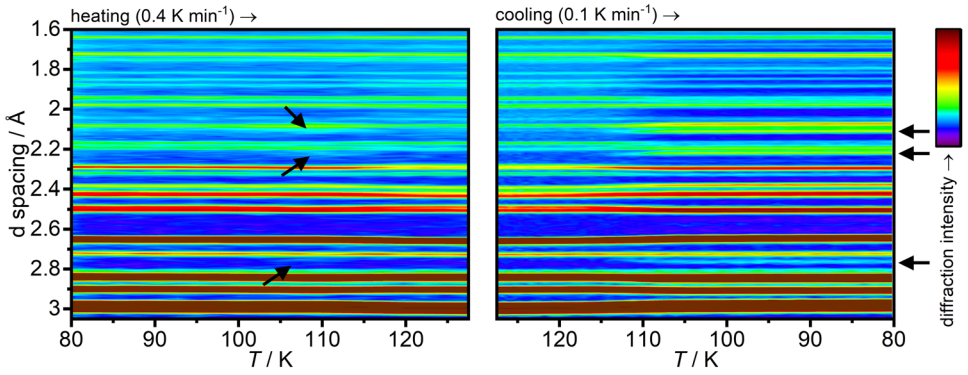

FIG. 4. Neutron diffraction data of a DCl-doped pressure-quenched ice V sample heated at ambient pressure from (left) 80–127 K at 0.4 K min^{-1} followed by (right) cooling back to 80 K at 0.1 K min^{-1}. Arrows highlight the Bragg peaks characteristic of ice XIII.

ordering explains why slow-cooling under pressure leads to a less ordered sample compared to cooling at ambient pressure since the pressure acts against the volume expansion upon ordering.

Structure of doped ice V before the phase transition to ice XIII

As mentioned earlier, ice V is a hydrogen-disordered phase of ice with some partial hydrogen order.[10] It is, therefore, interesting to ask the question if the partial order in ice V just above the phase transition temperature to ice XIII differs if different dopants are used. Lobban *et al.* described the partial hydrogen order in ice V using four order parameters that reflect the occupancies of the various deuterium sites (see Table I).[10] The relationships of the order parameters with the occupancies of the various hydrogen sites are given in Table II. For a pure ice V sample at 127 K and ambient pressure, they found $\alpha = 0.398$, $\beta = 0.189$, $\gamma = 0.564$, and $\delta = 0.850$. The quite pronounced deviations of β and δ from $\frac{1}{2}$ highlight the partial order present in this phase of ice. Table I also shows the order parameters for the various doped ice V samples at ~130 K as determined by Rietveld refinement using the $A2/a$ crystallographic model of ice V. There are no pronounced differences between the doped and the pure samples, which is also consistent with the lattice constants of the ice V samples shown in Figs. 3(a)–3(d). If anything, judging from the order parameters, the DCl-doped ice V may be slightly more ordered than the others. Calorimetrically, the orientational glass transition of pure ice V has been found at around 130 K.[16,21] This means that pure ice V at 127 K is not far out of equilibrium, and the order parameters are, therefore, similar compared to the doped samples. The full crystal structure information of DCl-doped ice V at 125 K is given in Table II.

Structure of ice XIII

The additional Bragg peaks that are observed for ice XIII and absent for ice V indicate a lowering of the space group symmetry upon hydrogen ordering without the need for changing the size of the unit cell.[15] Specifically, the additional Bragg peak at ~2.76 Å can be indexed as the 31-$\bar{2}$ reflection, the peaks at ~2.22 Å as 123 and 032, and finally, the peaks at ~2.07 Å as 114 and 132. The highest symmetry space group that meets the reflection conditions is $P2_1/a$, which is also the space group discussed by Kamb in an abstract for the hydrogen-ordered counterpart of ice V.[33] It is noted that $P2_1/c$ would be the corresponding standard setting. However, in keeping with the widely used $A2/a$ setting used for ice V,[3,10] we maintain the corresponding setting for ice XIII.

TABLE I. Order parameters as defined in Ref. 10 of the deuterium sites of doped and pure ice V samples. All samples were characterized at ambient pressure. Heating and cooling was carried out at ambient pressure unless specified otherwise.

Dopant	T (K)	Sample history	α	β	γ	δ
DCl	130	Heated from 80 K	0.435(4)	0.136(3)	0.525(2)	0.883(3)
DF	80	Cooled at 0.8 K min^{-1} at 0.5 GPa	0.464(5)	0.082(4)	0.529(4)	0.928(3)
DF	128	Heated from 80 K	0.421(4)	0.164(4)	0.549(3)	0.862(3)
DF	80	Cooled at 0.2 K min^{-1}	0.467(7)	0.112(6)	0.514(6)	0.912(5)
KOD	80	Cooled at 0.8 K min^{-1} at 0.5 GPa	0.417(5)	0.139(4)	0.528(4)	0.917(3)
KOD	131	Heated from 80 K	0.418(4)	0.179(4)	0.551(4)	0.867(3)
KOD	80	Cooled at 0.2 K min^{-1}	0.412(5)	0.155(4)	0.551(4)	0.895(3)
LiOD	80	Cooled at 0.1 K min^{-1}	0.424(2)	0.071(2)	0.545(2)	0.893(2)
Pure[10]	127	Quenched	0.398(10)	0.189(12)	0.564(8)	0.850(12)
Pure[10]	98	Quenched	0.419(9)	0.227(10)	0.536(6)	0.819(10)

TABLE II. Wyckoff positions, fractional atomic coordinates, fractional occupancies, order parameters, and isotropic atomic-displacement parameters (U_{iso}) of DCl-doped D_2O ice V at 125 K and ambient pressure. The space group is *A2/a*. The lattice constants are: a = 9.192 56(10) Å, b = 7.521 47(11) Å, c = 10.310 17(11) Å, and β = 109.3174(9). Numbers in parentheses are statistical errors of the last significant digit(s) of refined quantities. The positions of the sites with low occupancies cannot be considered to be accurate and are, therefore, given without error. The order parameters of the deuterium sites are as defined in Ref. 10.

Atom label	Wyckoff position	Atom type	x	y	z	Occupancy	Order parameter	U_{iso}* 100
O(1)	4e	O	0.250 000	0.816 99(65)	0.000 000	1.0000	...	2.348(32)
O(2)	8f	O	0.460 37(30)	0.055 79(35)	0.155 62(24)	1.0000	...	2.348(32)
O(3)	8f	O	0.276 47(29)	0.651 29(36)	0.247 60(32)	1.0000	...	2.348(32)
O(4)	8f	O	0.397 98(27)	0.359 07(37)	0.985 4(27)	1.0000	...	2.348(32)
D(5)	8f	D	0.335 21(50)	0.895 71(56)	0.046 23(39)	0.565(4)	$1-\alpha$	3.00(4)
D(6)	8f	D	0.245 10(55)	0.746 79(63)	0.078 64(81)	0.435(4)	α	3.00(4)
D(7)	8f	D	0.401 03(68)	0.963 03(81)	0.092 34(58)	0.435(4)	α	3.00(4)
D(8)	8f	D	0.416 796	0.091 464	0.216 554	0.136(2)	β	3.00(4)
D(9)	8f	D	0.466 99(45)	0.159 77(55)	0.103 98(42)	0.525(3)	γ	3.00(4)
D(10)	8f	D	0.561 95(28)	0.003 29(28)	0.195 66(23)	0.883(2)	δ	3.00(4)
D(11)	8f	D	0.253 58(44)	0.703 89(62)	0.155 03(59)	0.565(4)	$1-\alpha$	3.00(4)
D(12)	8f	D	0.352 761	0.555 271	0.260 564	0.117(2)	$1-\delta$	3.00(4)
D(13)	8f	D	0.318 60(68)	0.736 89(93)	0.320 39(70)	0.475(3)	$1-\gamma$	3.00(4)
D(14)	8f	D	0.182 57(31)	0.612 65(37)	0.261 35(24)	0.864(2)	$1-\beta$	3.00(4)
D(15)	8f	D	0.435 70(57)	0.262 81(79)	0.047 83(54)	0.475(3)	$1-\gamma$	3.00(4)
D(16)	8f	D	0.305 40(42)	0.388 64(49)	0.000 35(49)	1/2	...	3.00(4)
D(17)	8f	D	0.365 00(53)	0.307 35(69)	0.896 71(61)	0.561(3)	γ	3.00(4)
D(18)	8f	D	0.467 76(47)	0.457 11(56)	0.995 68(50)	1/2	...	3.00(4)

The reduction in space group symmetry from $A2/a$ to $P2_1/a$ goes along with the loss of two-fold rotational axes and some of the inversion centers. This then results in Wyckoff splitting of all atomic positions apart from the O(1) position, which is the only one with a multiplicity of 4 and on a special position in the ice V structure. All other oxygen and hydrogen positions have multiplicities of 8 in ice V, which split into two sets of general positions in ice XIII with multiplicities of 4. Because of the way the Wyckoff splitting works, the D(16) and D(18) positions in ice V are no longer required to have $\frac{1}{2}$ occupancies, which means that $P2_1/a$ permits full hydrogen order. In total, there are seven distinct oxygen and 28 hydrogen sites in ice XIII. In a fully ordered structure, 14 of the hydrogen sites must be occupied and 14 empty.

Starting off from a completely hydrogen-disordered $P2_1/a$ structure, the crystal structure of ice XIII was refined using the diffraction data of the slow-cooled DCl-doped sample at 12 K. The Rietveld fit is shown in Fig. 5(a), and the crystal structure information is given in Table III, which is in good agreement with the structure at 80 K reported in Ref. 15. The refined fractional occupancies indicate a highly hydrogen-ordered structure with an average deviation of the occupancies from full hydrogen order of about 4.7%.

The experimental structure of ice XIII is one out of 35 hydrogen-ordered configurations possible in $P2_1/a$ as determined by graph invariant theory.[23] Unfortunately, the details of the 35 configurations were not given in Ref. 23. We, therefore, produced the possible hydrogen-ordered configurations in $P2_1/a$ by using a simple self-written computer program that systematically goes through the permutations of occupied and empty hydrogen sites, and saves all structures that obey the ice rules. Using this approach, 70 different configurations were obtained. However, upon closer inspection, it was found that two structures always give the same diffraction data and are, hence, symmetrically equivalent yielding overall the 35 possible configurations mentioned earlier. The symmetry relationship between the pairs of equivalent structures was found to be a translation half-way along the c direction. The occupancies of the hydrogen sites of the 35 configurations are given in Table IV.

To gain further confidence in the crystal structure of ice XIII, all 35 configurations were refined against the experimental diffraction data. The resulting χ^2 parameters, which reflect the goodness of the fits, are shown in Fig. 6. Configuration 4, which corresponds to the previously determined structure, gives the best fit to the diffraction data out of all 35 configurations. It is interesting to note that configurations 11, 12, and 33 also gave quite good fits. However, upon inspection of the resulting structures, highly unrealistic O–D bond distances were found.

Only configurations 1–5 correspond to structures that agree with the tendencies of the β and δ order parameters in ice V to move toward zero and one, respectively.[10] So, even ignoring the disintegrated molecules in configurations 11, 12, and 33, configuration 4 is the only one that gives a good fit to the diffraction data and maintains the partial hydrogen order already established in ice V. This fact is illustrated in Fig. 7, where the fractional occupancies of ice XIII are plotted for the various hydrogen sites together with the corresponding occupancies of ice V. In principle, the nature of the hydrogen order of ice XIII could be

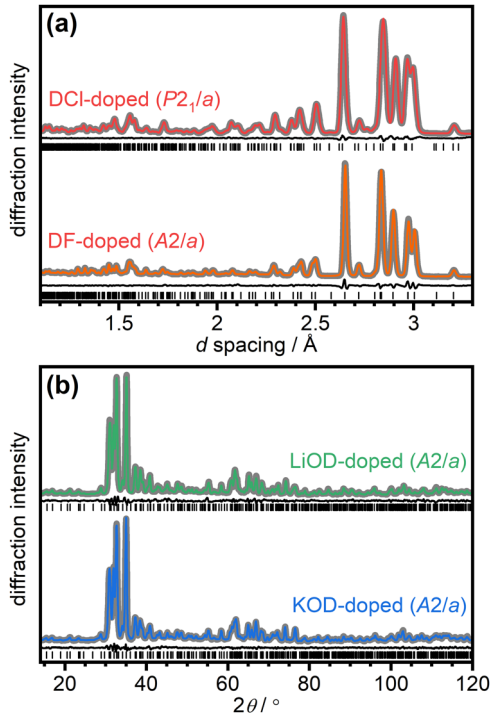

FIG. 5. Rietveld fits to the diffraction data of various doped ice V/XIII samples after slow-cooling at ambient pressure. Time-of-flight and constant-wavelength neutron diffraction data are shown in (a) and (b), respectively. The experimental data are shown as thick gray lines and the Rietveld fits as thinner colored lines. Black lines underneath the diffraction data show the residuals, and the tick marks indicate the positions of the Bragg peaks. The $P2_1/a$ structural model of ice XIII was used to fit the diffraction data of the DCl-doped sample, whereas the $A2/a$ model was used for the other three patterns. The diffraction data of the DCl-doped sample were collected at 12 K, whereas the other patterns were recorded at 80 K.

described with eight order parameters. However, the comparison with ice V would then become quite cumbersome, and we, therefore, prefer to simply show the occupancies of all hydrogen sites. The gray-shaded areas in Fig. 7 highlight the pairs of hydrogen positions that are symmetry-equivalent in ice V. All hydrogen positions that are related to the α and γ order parameters, which are close to $\frac{1}{2}$ in ice V, split into one occupied and one empty site in ice XIII. The positions related to the β and δ order parameters, which are already approaching either occupied or empty states, complete these trends, meaning that both sites become either occupied or empty. Given that there must be energetic reasons for the partial hydrogen order in ice V, it makes sense that these structural trends are perpetuated into ice XIII.

Consistent with the changes in the lattice constants discussed earlier, the fractional occupancies of the DCl-doped sample slow-cooled at 0.5 GPa show less hydrogen order compared to the sample slow-cooled at ambient pressure. The average deviation from full hydrogen order is 11.4%. However, only the hydrogen positions related to the α and γ order parameters are more disordered. The hydrogen positions related to β and δ display very similar degrees of hydrogen order independent of whether the sample was slow-cooled at 0.5 GPa or ambient pressure. In other words, the positions that are already quite ordered in ice V order well in ice XIII independent of the pressure. It would be intriguing to relate this phenomenon to the structural characteristics of ice XIII or the changes in the lattice constants discussed earlier. However, at present, we have not been successful in identifying a structural origin for this finding.

In a next step, it was investigated if other space groups are possible for ice XIII. For this analysis, the conventional settings of the monoclinic space groups are used. This means that $C2/c$ was used as the space group for ice V to search for subgroups. Keeping the same size of the unit cell, the possible subgroups of $C2/c$ are $P2_1/c$ (corresponding to the previously discussed $P2_1/a$ structure), $P2_1/n$, P_2/c, $P2/n$, Cc, $C2$, and $P-1$. In all cases, the number of hydrogen positions increase from 14 to 28. The number of oxygen positions increases from 4 to either 7 ($P2_1/c$, $P2_1/n$, Cc, and $P\bar{1}$) or 8 (P_2/c, $P2/n$, and $C2$). All structures are non-polar apart from Cc and $C2$. The Cc, $C2$, and $P\bar{1}$ space groups can be excluded right away because they do not allow the 31-$\bar{2}$ Bragg peak characteristic of ice XIII. Furthermore, $C2$ and $P\bar{1}$ display two symmetry-equivalent hydrogen positions along the same hydrogen bond, which means that full hydrogen order is not permitted in these space groups. The fractional occupancies along these hydrogen bonds are restricted to $\frac{1}{2}$. The distinction between $P2_1/c$, $P2_1/n$, P_2/c, and $P2/n$ is somewhat less straightforward. The experimental diffraction data of ice XIII displays a weak 10-$\bar{2}$ Bragg peak at around 4.59 Å, which is not allowed in $P2_1/n$ and $P2/n$. In addition, $P2_1/n$, P_2/c and $P2/n$, $P2_1/c$ contain hydrogen bonds with two symmetry-equivalent hydrogen positions. This means that $P2_1/c$ and the previously used corresponding $P2_1/a$ structure are the only options capable of reproducing the new Bragg peaks of ice XIII and permitting full hydrogen order. All of the above space groups have further subgroups of course. For example, the subgroups of $P2_1/c$ are Pc, $P2_1$, and $P\bar{1}$, which would all yield 70 different atomic positions within the same size of the unit cell. The refinement of these structures using powder diffraction data would represent a major challenge. However, it needs to be stressed that the $P2_1/a$ model provides an excellent fit to the experimental diffraction data. There is, therefore, no reason to assume that the space group symmetry should be lower than $P2_1/a$.

Partially hydrogen-ordered samples

The structural refinements related to the partially ordered ice XIII samples represent their own set of challenges. The key question is when the space group should change from $A2/a$ to $P2_1/a$. In the absence of the Bragg peaks characteristic of ice XIII, it was decided to use the $A2/a$ structural model for the diffraction data of the DF-, LiOD-, and KOD-doped samples slow-cooled at ambient pressure, as shown in Figs. 5(a) and 5(b). The refined order parameters of those samples at 80 K are given in Table I. In line with the changes in the lattice constants, the DF-doped sample appears to be the most ordered. The residuals of the fit of the DF-doped sample show a few sharp spikes (e.g., at 54.8°), which could be taken as an indication that the $A2/a$ model is on the verge of failing.

TABLE III. Wyckoff positions, fractional atomic coordinates, fractional occupancies, order parameters, and isotropic atomic-displacement parameters (U_{iso}) of D_2O ice XIII at 12 K and ambient pressure. The space group is $P2_1/a$. The lattice constants are: a = 9.240 33(13) Å, b = 7.462 35(11) Å, c = 10.291 66(13) Å, and β = 109.7675(10). Numbers in parentheses are statistical errors of the last significant digit(s) of refined quantities. The positions of the sites with low occupancies cannot be considered to be accurate and are, therefore, given without error.

Atom label	Wyckoff position	Atom type	x	y	z	Occupancy	U_{iso}* 100
O(1)	4e	O	0.253 4(6)	0.563 9(5)	0.252 0(5)	1.0000	1.082(32)
O(2)	4e	O	0.477 7(6)	0.799 0(5)	0.408 1(5)	1.0000	1.082(32)
O(3)	4e	O	0.051 2(5)	0.806 9(5)	0.094 6(5)	1.0000	1.082(32)
O(4)	4e	O	0.260 5(4)	0.403 6(6)	0.499 6(5)	1.0000	1.082(32)
O(5)	4e	O	0.211 1(4)	0.405 3(5)	0.003 1(5)	1.0000	1.082(32)
O(6)	4e	O	0.417 0(4)	0.111 7(6)	0.233 9(4)	1.0000	1.082(32)
O(7)	4e	O	0.126 1(5)	0.113 5(6)	0.265 2(4)	1.0000	1.082(32)
D(8)	4e	D	0.344 38(40)	0.640 1(4)	0.301 36(32)	0.972(5)	1.543(24)
D(9)	4e	D	0.167 800	0.641 700	0.207 800	0.035(5)	1.543(24)
D(10)	4e	D	0.244 21(45)	0.495 5(5)	0.330 01(46)	0.939(5)	1.543(24)
D(11)	4e	D	0.253 700	0.504 700	0.173 700	0.019(5)	1.543(24)
D(12)	4e	D	0.401 300	0.728 700	0.345 200	0.028(5)	1.543(24)
D(13)	4e	D	0.107 28(41)	0.715 3(5)	0.156 25(39)	0.965(5)	1.543(24)
D(14)	4e	D	0.422 500	0.809 500	0.468 400	0.011(4)	1.543(24)
D(15)	4e	D	0.077 500	0.809 500	0.031 600	0.005(4)	1.543(24)
D(16)	4e	D	0.483 22(42)	0.905 6(5)	0.357 51(36)	0.947(5)	1.543(24)
D(17)	4e	D	0.028 000	0.911 300	0.150 800	0.055(4)	1.543(24)
D(18)	4e	D	0.577 29(47)	0.750 9(5)	0.444 10(39)	0.949(6)	1.543(24)
D(19)	4e	D	0.949 43(54)	0.751 3(5)	0.048 56(38)	0.998(5)	1.543(24)
D(20)	4e	D	0.248 200	0.445 800	0.406 200	0.061(5)	1.543(24)
D(21)	4e	D	0.238 31(35)	0.455 0(4)	0.099 25(39)	0.981(5)	1.543(24)
D(22)	4e	D	0.355 600	0.305 400	0.522 500	0.051(6)	1.543(24)
D(23)	4e	D	0.144 400	0.305 400	0.977 500	0.002(5)	1.543(24)
D(24)	4e	D	0.303 42(40)	0.490 3(6)	0.577 59(43)	0.885(5)	1.543(24)
D(25)	4e	D	0.168 800	0.484 700	0.932 700	0.066(5)	1.543(24)
D(26)	4e	D	0.168 67(40)	0.356 2(6)	0.512 94(38)	0.989(4)	1.543(24)
D(27)	4e	D	0.307 61(42)	0.372 9(6)	0.991 32(33)	0.995(4)	1.543(24)
D(28)	4e	D	0.437 300	0.019 300	0.304 300	0.053(5)	1.543(24)
D(29)	4e	D	0.078 04(40)	0.019 6(6)	0.198 31(38)	0.945(4)	1.543(24)
D(30)	4e	D	0.324 18(44)	0.137 0(5)	0.254 03(47)	0.919(5)	1.543(24)
D(31)	4e	D	0.200 800	0.139 200	0.255 200	0.081(5)	1.543(24)
D(32)	4e	D	0.381 02(45)	0.048 9(5)	0.146 35(46)	0.934(5)	1.543(24)
D(33)	4e	D	0.130 700	0.062 300	0.349 300	0.115(5)	1.543(24)
D(34)	4e	D	0.467 300	0.197 300	0.228 700	0.071(6)	1.543(24)
D(35)	4e	D	0.050 16(39)	0.208 3(5)	0.253 32(43)	0.929(6)	1.543(24)

As previously found with Raman spectroscopy,[22] the degree of hydrogen order of the slow-cooled KOD-doped sample is close to pure ice V. This illustrates that the irreversible endotherm found upon heating such a sample[18,21] is an overshoot relaxation feature related to the underlying glass transition and not due to a reversible transition from hydrogen order to hydrogen disorder. In other words, the enthalpy of such a peak in calorimetry is not latent, and it is, therefore, not possible to relate it to changes in entropy.

Transient ordering in calorimetry

In a final step, it was investigated if the transient ordering phenomenon can be found in calorimetry as well. Based on the insights gained earlier, it should be possible to obtain the most disordered HCl-doped sample by quenching ice V at the highest possible pressure. As shown in Figs. 1(a) and 1(b), the low-temperature metastability region of ices XIII/V was mapped up to 2.5 GPa. Figure 8 shows DSC data of HCl-doped samples slow-cooled at 0.5 GPa and quenched at 1.6 and 2.5 GPa. The slow-cooled sample is expected to be quite hydrogen-ordered and, therefore, only shows an endotherm upon heating corresponding to the ice XIII to ice V phase transition. The high-pressure-quenched samples on the other hand, which should be less ordered, indeed, display exothermic transient ordering features followed by the endotherm corresponding to hydrogen disordering. As expected for a more disordered sample, the transient ordering exotherm is more pronounced for the sample quenched at

TABLE IV. Possible hydrogen-ordered configurations for the space group $P2_1/a$ with the hydrogen sites either empty (0) or occupied (1). Out of the 70 possibilities, only the 35 symmetrically distinct configurations are shown. Configurations 1–5 are in accordance with the partial hydrogen order of ice V, and configuration 4 corresponds to the experimentally found structure of ice XIII.

Nos.	D8	D9	D10	D11	D12	D13	D14	D15	D16	D17	D18	D19	D20	D21	D22	D23	D24	D25	D26	D27	D28	D29	D30	D31	D32	D33	D34	D35
1	0	0	1	1	1	1	0	0	0	0	1	1	0	0	0	0	1	1	1	1	1	1	1	0	0	0	0	1
2	1	0	0	1	0	1	0	0	1	0	1	1	1	0	0	0	0	1	1	1	0	1	1	0	0	1	1	0
3	1	0	1	0	0	1	0	0	1	0	1	1	0	1	0	0	1	0	1	1	0	1	0	1	1	0	1	0
4	1	0	1	0	0	1	0	0	1	0	1	1	0	1	0	0	1	0	1	1	0	1	1	0	1	0	0	1
5	1	1	0	0	0	0	0	0	1	1	1	1	1	1	0	0	0	0	1	1	0	0	1	0	1	1	0	1
6	1	0	0	1	0	1	0	0	1	1	1	0	1	0	0	1	0	0	1	1	0	0	0	1	1	1	1	0
7	1	0	0	1	0	1	0	0	1	1	1	0	1	0	0	1	0	0	1	1	0	0	1	0	1	1	0	1
8	0	0	1	1	1	1	0	0	1	0	0	1	0	0	1	0	0	1	1	1	0	1	1	0	0	1	1	0
9	0	0	1	1	1	1	0	0	1	1	0	0	0	0	1	1	0	0	1	1	0	0	1	0	1	1	0	1
10	1	0	0	1	0	1	0	1	1	0	1	0	1	0	0	1	0	1	1	0	0	1	1	0	0	1	1	0
11	1	0	1	0	0	1	0	1	1	0	1	0	0	1	0	1	1	0	1	0	0	1	0	1	1	0	1	0
12	1	0	1	0	0	1	0	1	1	0	1	0	0	1	0	1	1	0	1	0	0	1	1	0	1	0	0	1
13	1	0	0	1	0	1	1	0	0	0	1	1	1	0	0	0	1	1	0	1	1	1	0	1	0	0	1	0
14	1	0	0	1	0	1	1	0	0	0	1	1	1	0	0	0	1	1	0	1	1	1	1	0	0	0	0	1
15	1	1	0	0	0	0	1	0	0	1	1	1	1	1	0	0	1	0	0	1	1	0	0	1	1	0	0	1
16	1	0	0	1	0	1	1	0	0	1	1	0	1	0	0	1	1	0	0	1	1	0	0	1	1	0	0	1
17	0	0	1	1	1	1	1	0	0	0	0	1	0	0	1	0	1	1	0	1	1	1	0	1	0	0	1	0
18	0	0	1	1	1	1	1	0	0	0	0	1	0	0	1	0	1	1	0	1	1	1	1	0	0	0	0	1
19	1	0	0	1	0	1	1	0	1	0	0	1	1	0	1	0	0	1	0	1	0	1	1	0	0	1	1	0
20	1	0	1	0	0	1	1	0	1	0	0	1	0	1	1	0	1	0	0	1	0	1	0	1	1	0	1	0
21	1	0	1	0	0	1	1	0	1	0	0	1	0	1	1	0	1	0	0	1	0	1	1	0	1	0	0	1
22	1	1	0	0	0	0	1	0	1	1	0	1	1	1	1	0	0	0	0	1	0	0	0	1	1	1	1	0
23	1	1	0	0	0	0	1	0	1	1	0	1	1	1	1	0	0	0	0	1	0	0	1	0	1	1	0	1
24	0	0	1	1	1	1	1	0	0	1	0	0	0	0	1	1	1	0	0	1	1	0	0	1	1	0	0	1
25	1	0	0	1	0	1	1	0	1	1	0	0	1	0	1	1	0	0	0	1	0	0	0	1	1	1	1	0
26	1	0	0	1	0	1	1	0	1	1	0	0	1	0	1	1	0	0	0	1	0	0	1	0	1	1	0	1
27	1	1	0	0	0	0	1	1	0	0	1	1	1	1	0	0	1	1	0	0	1	1	1	0	0	0	0	1
28	1	0	0	1	0	1	1	1	0	0	1	0	1	0	0	1	1	1	0	0	1	1	0	1	0	0	1	0
29	1	0	0	1	0	1	1	1	0	0	1	0	1	0	0	1	1	1	0	0	1	1	1	0	0	0	0	1
30	1	1	0	0	0	0	1	1	1	0	0	1	1	1	1	0	0	1	0	0	0	1	1	0	0	1	1	0
31	0	0	1	1	1	1	1	1	0	0	0	0	0	0	1	1	1	1	0	0	1	1	1	0	0	0	0	1
32	1	0	0	1	0	1	1	1	1	0	0	0	1	0	1	1	0	1	0	0	0	1	1	0	0	1	1	0
33	1	0	1	0	0	1	1	1	1	0	0	0	0	1	1	1	1	0	0	0	0	1	0	1	1	0	1	0
34	1	0	1	0	0	1	1	1	1	0	0	0	0	1	1	1	1	0	0	0	0	1	1	0	1	0	0	1
35	1	1	0	0	0	0	1	1	1	1	0	0	1	1	1	1	0	0	0	0	0	0	1	0	1	1	0	1

2.5 GPa compared to quenching at 1.6 GPa. Using the slowest possible heating rate of 2.5 K min^{-1} with our calorimeter is expected to enhance the exotherms since a maximal period of time is spent in the temperature range where the transient ordering takes place. The areas of the endotherms that follow are smaller compared to the slow-cooled sample, indicating a lower degree of hydrogen disorder in the quenched materials. However, it needs to be stressed that the areas of endotherms would be even smaller if the transient ordering had not taken place. Since the transient ordering is irreversible, changes in entropy cannot be obtained.

In summary, with the demonstration that transient ordering is not only observed for ices VI/XV[26,31] but also for ices V/XIII, it

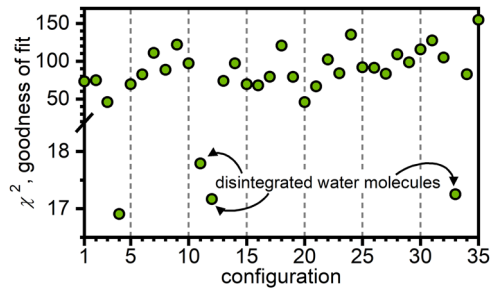

FIG. 6. Testing the fits of the 35 possible fully hydrogen-ordered configurations of $P2_1/a$ to the diffraction data of the most hydrogen-ordered ice XIII recorded after slow-cooling at ambient pressure. Only configurations 1–5 are consistent with the partial hydrogen order that exists in ice V before the phase transition to ice XIII with configuration 4 giving the best fit to the data. Three more configurations fit the diffraction data well. However, the refined structures include water molecules with highly unrealistic intermolecular bond distances.

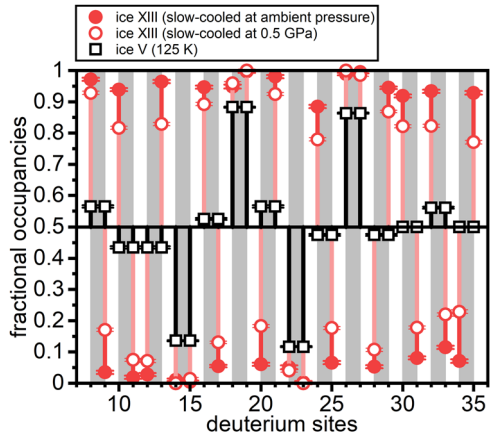

FIG. 7. Fractional occupancies of the deuterium sites of $P2_1/a$ ice XIII after slow-cooling at 0.5 GPa (open circles) and at ambient pressure (full circles). The open squares show the corresponding fractional occupancies of ice V at 125 K. The gray-shaded areas indicate the pairs of positions that are symmetry-equivalent in ice V.

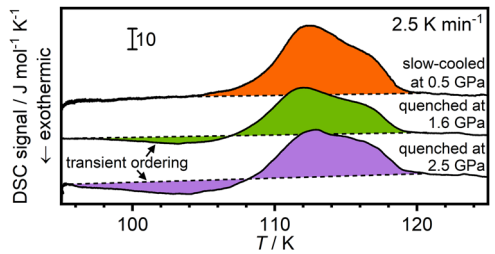

FIG. 8. Differential scanning calorimetry of DCl-doped ice V/XIII samples slow-cooled at 0.5 GPa and quenched at 1.6 and 2.5 GPa. The samples were heated at 2.5 K min^{-1} at ambient pressure.

seems plausible that this phenomenon could in principle be possible for all phases of ice if they are metastable with respect to more hydrogen-ordered states and if the ordering kinetics are sufficiently fast. Translated into the language of glasses, the transient ordering can be described as the crystallization of the glassy state, which is only orientational in our case, followed by melting up further heating.

CONCLUSIONS

Changes in the lattice constants during the reversible ice V to ice XIII phase transition were found to be highly sensitive indicators for the extent of order in ice XIII. This approach appears to be more sensitive than the appearance of the Bragg peaks characteristic of ice XIII, which were only observed for the most highly ordered samples. Anisotropic behavior in the changes of the lattice constants was observed with some lattice constants contracting and others expanding during the phase transition. For the DCl-, DF-, and LiOD-doped samples, identical trends in the changes were observed, suggesting that all three dopants enable similar ordering processes albeit with different kinetics. KOH doping was not found to induce significant hydrogen order.

The previously suggested space group of ice XIII, $P2_1/a$, was scrutinized, and it was found that this is the only subgroup of the ice V $A2/a$ space group that permits the new Bragg peaks characteristic of ice XIII and allows complete hydrogen order. All 35 possible hydrogen-ordered configurations in $P2_1/a$ were tested, and the previously determined structure, which was obtained from a free refinement of the hydrogen-disordered structure, was confirmed. Only five of the 35 configurations are consistent with the partial hydrogen order that already exists in ice V, and the experimental structure was found to be one of them. This means that the partial hydrogen order present in ice V is carried forward into ice XIII and very close to complete order is achieved for those positions. The kinetics of these ordering processes were found to be essentially pressure independent in the 0–0.5 GPa range, whereas the other hydrogen sites ordered more easily upon slow-cooling at ambient pressure. The slower kinetics of hydrogen ordering under pressure can be explained by a small increase in the volume of the unit cell upon hydrogen ordering. Finally, a pressure-quenched DCl-doped sample displayed significant "transient ordering" upon heating at ambient pressure as seen from the lattice constants. Based on the insight that pressure suppresses the hydrogen ordering, the transient ordering could now also be observed in calorimetry for HCl-doped H_2O samples pressure-quenched at 1.6 or 2.5 GPa. Together with previous observations for ices VI/XV, the transient ordering now observed for ices V/XIII suggests that this may be a general phenomenon for the ice phases that becomes observable below the hydrogen disordering temperature when metastable hydrogen-disordered states are heated and the hydrogen-ordering kinetics are sufficiently fast. If ices V/XIII can display endothermic peaks before the transient ordering exotherm, as observed for ices VI/XV,[31,32] will be the focus of future investigations.

Given the complex structural nature of ices V/XIII and the unusual fact that hydrogen ordering can be achieved with both acid and base dopants, this material is a particularly interesting test case for further investigations into the phenomenon of hydrogen ordering and defect dynamics in ice. The role of the dopant can, thereby,

be broken down into two different contributions. As a short-range effect, the anions and cations of the acid and base dopants are expected to only influence the local electric field and to change the polarizability of the neighboring water molecules. The migrating H_3O^+ or OH^- point defects, on the other hand, are thought to influence the structure and dynamics of ice over much longer distances, and as such, they appear to be the driving force behind the hydrogen-ordering processes.

ACKNOWLEDGMENTS

We thank the ISIS facility and the Institute Laue Langevin for access to neutron diffraction, and Ron Smith and Emmanuelle Suard for help with the neutron diffraction experiments. We are grateful to the late Erwin Mayer for his contributions during the early stages of this project.

DATA AVAILABILITY

Some of the raw data were generated at the ISIS and Institute Laue Langevin large scale facilities. The data that support the findings of this study and other data collected in our lab are available from the corresponding author upon reasonable request.

REFERENCES

[1] G. Tammann, Ann. Phys. **307**, 1 (1900).
[2] P. W. Bridgman, Proc. Am. Acad. Arts Sci. **47**, 441 (1912).
[3] B. Kamb, A. Prakash, and C. Knobler, Acta Crystallogr. **22**, 706 (1967).
[4] C. G. Salzmann, P. G. Radaelli, B. Slater, and J. L. Finney, Phys. Chem. Chem. Phys. **13**, 18468 (2011).
[5] J. E. Bertie and E. Whalley, J. Chem. Phys. **40**, 1646 (1964).
[6] G. J. Wilson, R. K. Chan, D. W. Davidson, and E. Whalley, J. Chem. Phys. **43**, 2384 (1965).
[7] E. Whalley and D. W. Davidson, J. Chem. Phys. **43**, 2148 (1965).
[8] W. C. Hamilton, B. Kamb, S. J. La Placa, and A. Prakash, in *Physics of Ice*, edited by N. Riehl, B. Bullemer, and H. Engelhardt (Plenum, New York, 1969), p. 44.
[9] W. F. Kuhs, C. Lobban, and J. L. Finney, Rev. High Pressure Sci. Technol. **7**, 1141 (1998).
[10] C. Lobban, J. L. Finney, and W. F. Kuhs, J. Chem. Phys. **112**, 7169 (2000).
[11] B. Minceva-Sukarova, G. E. Slark, and W. F. Sherman, J. Mol. Struct. **143**, 87 (1986).
[12] G. P. Johari and E. Whalley, J. Chem. Phys. **115**, 3274 (2001).
[13] L. Pauling, J. Am. Chem. Soc. **57**, 2680 (1935).
[14] H. Tran, A. V. Cunha, J. J. Shephard, A. Shalit, P. Hamm, T. L. C. Jansen, and C. G. Salzmann, J. Chem. Phys. **147**, 144501 (2017).
[15] C. G. Salzmann, P. G. Radaelli, A. Hallbrucker, E. Mayer, and J. L. Finney, Science **311**, 1758 (2006).
[16] C. G. Salzmann, I. Kohl, T. Loerting, E. Mayer, and A. Hallbrucker, Phys. Chem. Chem. Phys. **5**, 3507 (2003).
[17] Y. Tajima, T. Matsuo, and H. Suga, Nature **299**, 810 (1982).
[18] Y. P. Handa, D. D. Klug, and E. Whalley, J. Phys., Colloq. **48**, C1-435 (1987).
[19] B. Minceva-Sukarova, G. Slark, and W. F. Sherman, J. Mol. Struct. **175**, 289 (1988).
[20] C. G. Salzmann, P. G. Radaelli, A. Hallbrucker, E. Mayer, and J. L. Finney, in *Physics and Chemistry of Ice*, edited by W. F. Kuhs (The Royal Society of Chemistry, Cambridge, 2007), p. 521.
[21] C. G. Salzmann, P. G. Radaelli, J. L. Finney, and E. Mayer, Phys. Chem. Chem. Phys. **10**, 6313 (2008).
[22] C. G. Salzmann, A. Hallbrucker, J. L. Finney, and E. Mayer, Phys. Chem. Chem. Phys. **8**, 3088 (2006).
[23] C. Knight and S. J. Singer, J. Chem. Phys. **129**, 164513 (2008).
[24] K. W. Köster, A. Raidt, V. Fuentes Landete, C. Gainaru, T. Loerting, and R. Böhmer, Phys. Rev. B **94**, 184306 (2016).
[25] A. Rosu-Finsen and C. G. Salzmann, J. Chem. Phys. **148**, 244507 (2018).
[26] J. J. Shephard and C. G. Salzmann, Chem. Phys. Lett. **637**, 63 (2015).
[27] C. G. Salzmann, B. Slater, P. G. Radaelli, J. L. Finney, J. J. Shephard, M. Rosillo-Lopez, and J. Hindley, J. Chem. Phys. **145**, 204501 (2016).
[28] A. C. Larsen and R. B. Von Dreele, *General Structure Analysis System* (University of California, 1985).
[29] C. G. Salzmann, P. G. Radaelli, E. Mayer, and J. L. Finney, Phys. Rev. Lett. **103**, 105701 (2009).
[30] Z. Sharif, J. J. Shephard, B. Slater, C. L. Bull, M. Hart, and C. G. Salzmann, J. Chem. Phys. **154**, 114502 (2021).
[31] A. Rosu-Finsen and C. G. Salzmann, Chem. Sci. **10**, 515 (2019).
[32] T. M. Gasser, A. V. Thoeny, L. J. Plaga, K. W. Köster, M. Etter, R. Böhmer, and T. Loerting, Chem. Sci. **9**, 4224 (2018).
[33] B. Kamb and S. J. La Placa, Trans. Am. Geophys. Union **55**, 1202 (1974).